ALMA Memo No. 374
Wide Field Imagings with
the Atacama Large Millimter/
Submillimeter Array

Koh-Ichiro Morita
Nobeyama Radio Observatory,
National Astronomical Observatory of Japan.
Nobeyama, Minamimaki, Minamisaku, Nagano 384-1305, Japan.
Email: morita@nro.nao.ac.jp

May 28, 2001

Abstract. Image quality of wide field observations with the ALMA has been studied with imaging simulations. Results of the simulations showed that antenna pointing errors are a serious problem for obtaining high quality images because they make a large error in visibilities in the central (u,v) hole estimated by mosaicing data processings. The ALMA Compact Array (ACA) with more than 10 smaller dishes (6-8m) can compensate this problem. However, a carefull treatment of adding the data measured with the ACA to the data from the ALMA is needed to obtain a significant improvement of imaging performances. The ACA with 6m antennas has better imaging performances than that of the ACA with 8 m antennas, although the difference between them is small for noisy cases. Another option to realize high fidelity images for large objects is to improve the pointing of some or all of the 12 m antennas.

1. Introduction

FWHM of the 12 m antenna of the Atacama Large Millimeter/Submillimeter Array (ALMA) is less than 20 arcsecond at the wavelength shorter than 1 mm. Sizes of many science targets for the ALMA exceed this scale and wide field imagings using multi-pointing aperture synthesis (mosaicing) will be highly demanded.

For such wide field imagings, Fourier informations at shorter baselines or single dish data are quite important to obtain high quality images. However, the (u,v) coverage of the ALMA has a (u,v) hole between zero spacing and the shortest measured interferometric spacing, which is about 16 m. Therefore, we cannot measure the Fourier information around baselines from 0 - 16 m directly. Figure 1 (a) clearly shows such a (u,v) hole at the center of a snapshot (u,v) coverage for ALMA E configuration designed by M. Yun and L. Kogan.

We can estimate visibilities from 0 - 6 m from single dish mapping data. Information of spacings between 4 m and 16 m is obtained implicitly via the Ekers and Rots scheme (Ekers and Rots, 1979). Cornwell et al. (1992) have argued that, using mosaicing observations with single dish data, we can estimate large scale structures even with a homogeneous array correctly. Figure 1 (b) shows a result of mosaicing simulations using a source model of M31 HII region with the ALMA E array shown in Figure 1 (a). Total power data was included in this result, but thermal noise and any antenna errors were not added in this simultaion. It is clear that image quality of the result is quite high. The dynamic range of is about 34,000 and the median fidelity is about 900.

Pointing errors of the 12 m antennas, however, could cause serious errors in estimated visibilities around the (u,v) hole. Although Cornwell et al (1992) already discussed this problem, we need to clarify the effect on the wide field imaging with actual array configuration plan for the ALMA.
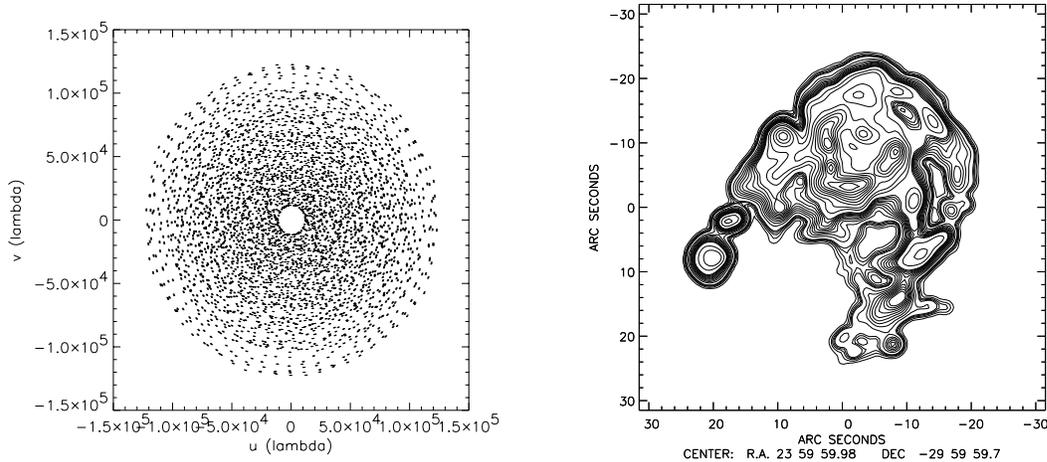
1

Figure 1. Left (a): A snapshot (u,v) coverage by a straw person plan of ALMA E configuration by M. Yun and L. Kogan. Right (b): A result of imaging simulation. Number of pointings is 7 × 7 and Frequency is assumed 230 GHz. Pointing separation was chosen to be $\lambda/2D$. Deconvolution algorithm was based on MEM. Contours = [-1, -0.8, -0.6, -0.4, -0.2, 0.2, 0.4, 0.6, 0.8, 1, 2, 3, 4, 5, 6, 7, 8, 9, 10, 15, 20, 30, 40, 50, 60, 70, 80, 90] %.

In recent discussion for an enhanced ALMA project, many people have proposed the ALMA Compact Array (ACA), which is an additional small array consisting of smaller dishes (6-8m), to solve the problem due to the central (u,v) hole (Yun, 2001). Such an array could compensate the problems, because we can measure the Fourier information in the (u,v) hole directly. Therefore, it is requested to see the merit of the ACA and to find the optimal design of the antenna diameter and the number of antennas.

For the above two purposes, we have conducted imaging simulations.

2. Imaging Simulation

Unfortunately, classical AIPS has no function to simulate mosaicing observations. Simulation capabilities of AIPS++ is under development, although it will have various functions for imaging simulations. Therefore, we have used SDE software system developed by T. Cornwell et al. for this study. There are many functions to simulate observations with noises and antenna errors developed by M. Holdaway in SDE.

2.1. Observing Parameters

The following imaging parameters have been used in the simulations:

ALMA Configuration	E configuration (proposed by M. Yun and L. Kogan)
Source Model	M31 HII region
Observing frequency	230 GHz
FWHM of the primary beam	∼ 22 × 22 arcsec.
Declination	-30 deg.
HA coverage	Snapshot (Integration time for each pointing = 1 min)
Number of Mosaicing pointings	7 × 7 (77 arcsec × arcsec)

2

Total power data were assumed to be measured by all 12 m antennas and ACA was used to observe visibilities of baselines only between the ACA antennas.

Following parameters in imaging process have been used in the simulations.

Imsize	128×128
Cellsize	0.5×0.5 arcsec
Convolution beam	1.6×1.6 arcsec Gaussian.

I have used an MEM based joint deconvolution program in SDE.

2.2. Error Analysis

In this report, we have used following parameters for error analysis.

Dynamic range (Off-source errors)

Select an off-source region, calculate the rms off source, divide that into the reconstructed peak. Off-source region was selected by setting pixels of the reference image below an appropriate level. The reference image was made from model image convolved with Gaussian beam used in deconvolution. In our simulations, we set 10^{-5} % of the peak as the clipping level.

Median fidelity index (On-source errors)

Make error (difference) image, make a mask for on-source regions based on the convolved model clipping below some level. Divide the absolute error into the pixel values of the convolved image. As some pixel errors will accidentally be very small, take the median of this fractional error image. The clipping level of 0.1 % of the peak was set in these simulations.

Visibility error

Make Fourier transform of the difference image and calculate its radial amplitude profile.

Relative visibility error

Visibility error normalized by Fourier transform of reference image.

3. Image Degradations due to Antenna Pointing Errors

The pointing error model used in these simulations is similar to that of T. Cornwell et al. (1992).

G	Global pointing offset: constant in time for the entire array.
I	Initial pointing offset: random among all antennas but constant in time
D	Drift: uniform among antennas and changes uniformly with time.
R	Random: is random among antennas and in time.

Acording to T. Cornwell et al., we have set these parameters following manner: G=(X,X), D=(X/2,0), I=(X,X), R=(X,X).

Figure 2 shows an example of these simulations of which pointing error is 6.1 % rms of primary beam width of the 12 m antenna. A large scale error is seen in the error image, which is caused by the pointing error.

The image degradations as a function of the pointing error for several SNR cases are shown in Figure 3. At 230 GHz band, we would expect to have a system temparture of 50 - 100 K. Assuming that the system tempature is 70 K and the antenna efficiency is 0.7, rms noise per baseline for snapshot (integration time = 1 min) and continuum (Bandwidth = 4GHz) observations is about 3.5 mJy. We used this rms noise level in the imaging simulations. In the case of 7×7 mosaicing, number of visibilities contributing to an imaging pixel in a mapping center is about 4400. Therefore, rms noise in image is about 0.05 m Jy / Beam.

The figure shows that pointing errors are a really serious problem for wide field imagings. For the case of no pointing error and noise free, we can easily obtain a very high quality image with the ALMA. However, a pointing error of only a few percent of the primary beam width makes a very large degradation of image quality. Current specification of pointing error for the ALMA 12 m antenna is 0.6 arcsec rms, which is ~ 3 % of the primary beam width at 230 GHz. Even

Freq (GHz)	115	230	350	630
Dynamic Range	> 1000	$700 \sim 800$	$400 \sim 500$	$300 \sim 400$
Fidelity Index	> 50	$20 \sim 30$	$10\sim 20$	< 10

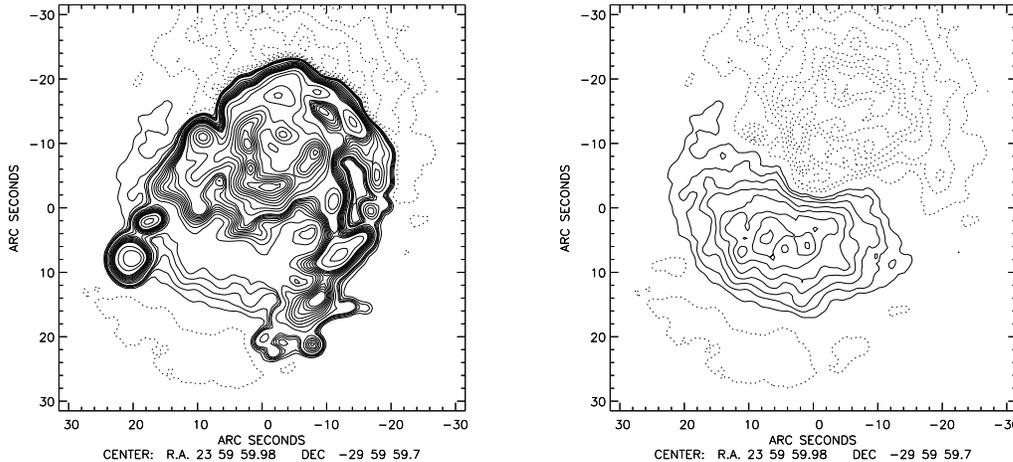Table 1.   The maximum achievable image qualities estimated from the simulations.

Figure 2.   Left (a): The deconvolved image for the pointing error with 6.1 % of primary beam width of 12 m atenna. CContours = [-1, -0.8, -0.6, -0.4, -0.2, 0.2, 0.4, 0.6, 0.8, 1, 2, 3, 4, 5, 6, 7, 8, 9, 10, 15, 20, 30, 40, 50, 60, 70, 80, 90] % The error distribution of the image in Figure 3. Right (b): Contour interval is 0.2 % of the peak.

if anomalous refraction does not exist, dynamic range decreases to less than 1,000 due to this pointing error for noise free cases.

In table 1, we show the maximum achievable image qualities predicted by the imaging simulations under the condition of the current specification.

Figure 4 shows radial profile of the relative visibility error for cases of several pointing errors. The simulations in this figure did not include any thermal noise. The figure indicates that the pointing error makes large imaging error which scales are almost consistent with the central (u,v) hole. Therefore, to compensate these imaging errors, we must reduce errors in estimated visibilities in the (u,v) hole.

4.   ALMA Compact Array

The ALMA Compact Array (ACA) which consists of smaller dishes (6-8m) has been proposed to solve the problems which are shown in previous section. To measure the Fourier information in the central (u,v) hole directly, the ACA would improve imaging performances of wide field observations with the ALMA.

4.1.   Array Configurations

To design array configurations for the ACA, it is important to obtain as many short baselines as possible. A hexagonal array is such a candidate. However antenna baseline vectors of a hexagonal array are too redundant and near sidelobe level is very high. After some simulations, we found that
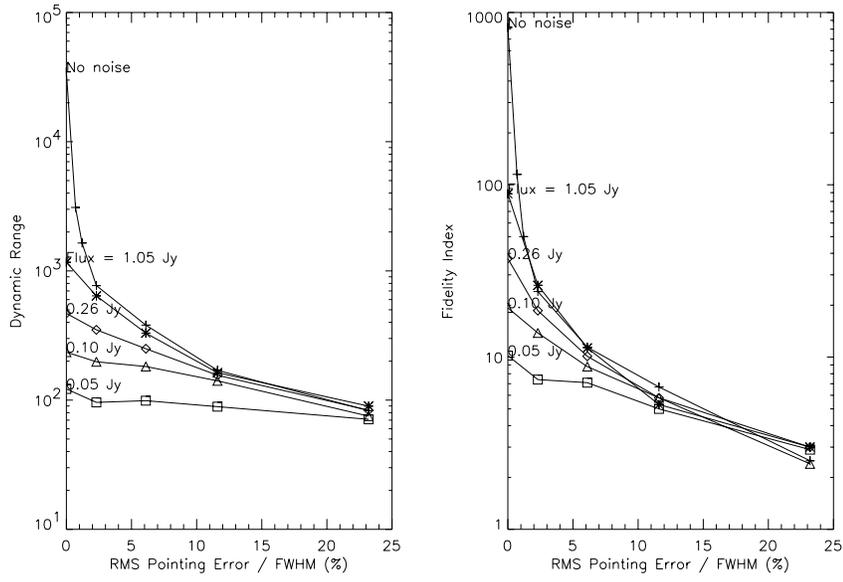
Figure 3.   The image degradations as a function of the pointing error for several SNR cases.
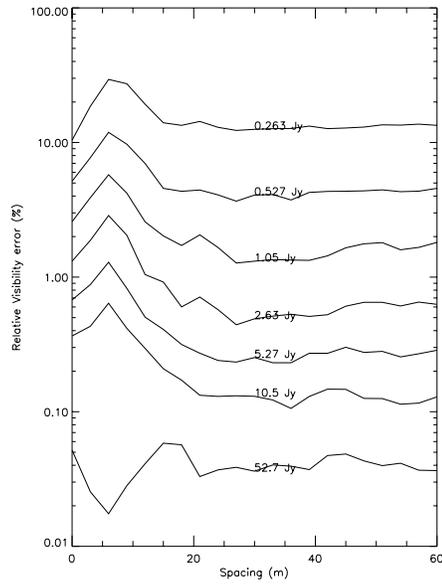

Figure 4.   Radial profile of the relative visibility error for several pointing errors.
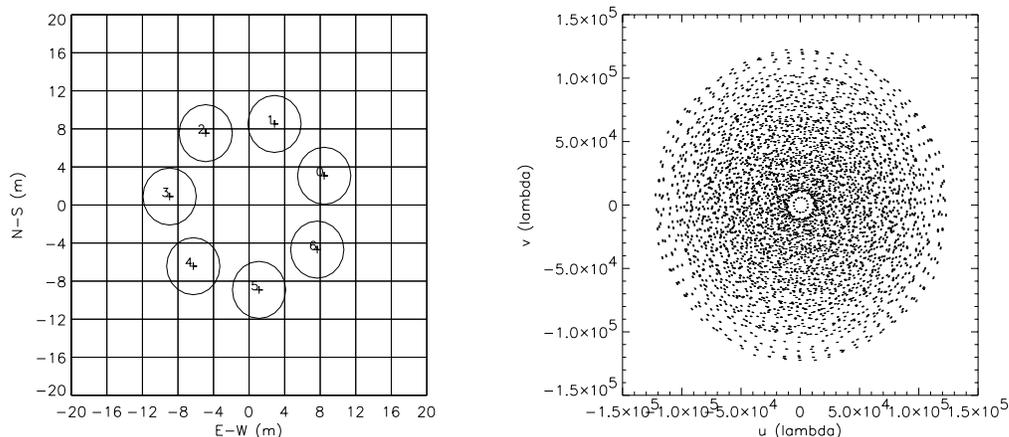
5

Figure 5. Array configuration of the ACA D6-7. A snapshot (u,v) coverage.

the performance of array configurations based on circular array design is superior to that based on a hexagonal array. Therefore, we selected several array configurations for the following simulations based on circular array design.

We selected 6 m and 8 m as antenna diameter of the ACA and the number of antennas was varied from 7 to 11. We also used 16 × 8 m array and 18 × 6 m array. For these arrays, we designed inner part based on the hexgonal concept and outer part based on the circular concept.

Array Name	D8-7	D8-9	D8-11	D8-16	D6-7	D6-9	D6-11	D6-18
Diameter	8 m	8 m	8 m	8 m	6 m	6 m	6 m	6m
Number of Antenna	7	9	11	16	7	9	11	18

Table 2. Configurations of the ACA used in the simulations.

Figure 5 shows the array configuration of D6-7 and it's snapshot (u,v) coverage.

4.2. Simulations including the ACA data

In the following simulations, we used only the ALMA interferometeric data, the ALMA total power data, and the ACA interferometric data for mosaicing image processings. We did not use cross correlation data between the ALMA and the ACA and the total power data from the ACA. These data have been considered to make no significant merit due to the sensitivity.

The angular separation between each pointing is λ/D, where D is an antenna diameter. We used 7×7 pointings for both mosaicing observations with the ALMA and the ACA. To scan almost same observing area with smaller dishes, we only need smaller number of pointings. Imaging simulations, however, clearly indicate that blank sky data are very important to reconstruct mosaicing data correctly. The ACA dishes have larger primary beam so that we need wider observing area than that of the ALMA.

The same pointing model and same rms pointing error as those of the 12 m antennas were used for the ACA antennas. In the following section, antenna pointing errors in all simulations are equal to 6.1 % of FWHM of the ALMA 12 m antenna. Of cource, the pointing accuracy of the ACA antenna could be smaller than that of the 12 m antenna. Since, however, the pointing

6

error due to anomalous refraction will be almost the same for the 12 m antenna and the 6 - 8 m antennas, this assumption may not be so different from the actual situation.

5. Effect of adding data from the ACA

5.1. The ALMA data + the ACA data

In Table 3, we show imaging qualities of simulation results including the ACA for noise free cases. In these simulations, we simply combined the ALMA interferometric data, the ALMA total power data, and ACA interferometric data. From the table, although fidelity index increases by adding the ACA data, dynamic range is almost same or less than that of the case of ALMA only. It is clear that simple addition of the ACA data does not make a significant improvement of imaging performances for wide field observations with the ALMA.

	ALMA only	D8-7	D8-11	D8-16	D6-7	D6-11	D6-18
Dynamic Range	381	370.	349	297	357.	346	293
Fidelity Index	11.4	11.4	14.0	14.7	15.0	16.0	22.5

Table 3.   Image qualities of simulation results using the ALMA data + the ACA data for noise free cases.

Table 4 shows similar results for the case including thermal noise. In this case, total flux of the object is assumed 0.26 Jy. These results indicate same tendency of noise free cases.

	ALMA only	D8-7	D8-11	D8-16	D6-7	D6-11	D6-18
Dynamic Range	250	246	242	227	249	250	241
Fidelity Index	10.1	10.3	11.6	12.9	10.8	11.3	13.1

Table 4.   Image qualities of simulation results using the ALMA data + the ACA data for noisy cases (Object flux = 0.26 Jy).

Radial profiles of visibility errors for noise free cases are shown in Figure 6. The figure indicates there are almost no improvement of visibility estimation in the central (u,v) hole. Since the ACA directly measures visibilities in the hole, these estimation errors are considered to be caused by the total power data measured with the 12 m antennas. Therefore, to improve reconstructed images, we need to reduce the contribution of the visibility estimation from the total power.

5.2. Smoothing the total power data from the 12 m antennas

As the discussion in previous section, low pass filtering of the total power data in spatial frequency space is considered to be efficient to improve the images from the ALMA data and the ACA. In this section, we show the simulation results using such a smoothed total power data. For low pass filtering, we convolved the total power data with a wider beam equivalent to that of 6 m antenna.

Table 5 shows the results for noise free cases. The image qualities increase by adding the ACA data. In particular, improvements of on-source errors (fidelities) are significant for most cases. Figure 7 shows radial profiles of visibility errors for the cases shown in Table 6. Significant improvements of the visibility estimation at the (u,v) hole are clearly shown in this figure. The reconstructed image and the error image for the case using the ACA D6-11 are shown in Figure 8 (a) and (b), respectively. Compared with Figure 1, Figure 2, and Figure 8, it is clear that this result is superior to that with the ALMA only.

Table 6 shows results for the same noisy cases as Table 4. The ACA improves the image quality for these cases, although these improvements are not so siginificant as the noise free cases.
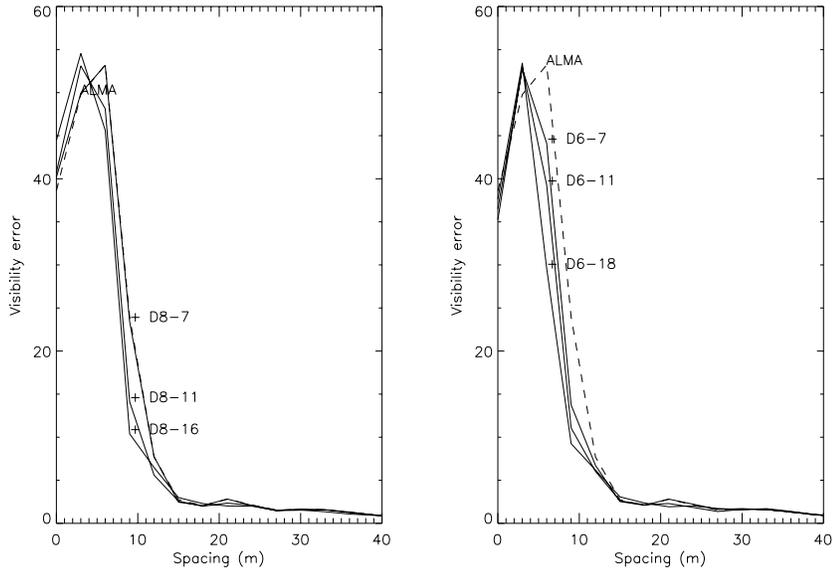
Figure 6.   Visibility error profile for noise free cases in Table 3.

	ALMA only	D8-7	D8-11	D8-16	D6-7	D6-11	D6-18
Dynamic Range	381	353	483	424	590	617	691
Fidelity Index	11.4	18.6	27.6	25.9	36.0	49.3	61.1

Table 5.   Image qualities of simulation results using smoothed total power data for noise free cases.

	ALMA only	D8-7	D8-11	D8-16	D6-7	D6-11	D6-18
Dynamic Range	250	258	338	305.	331.	322.	318.
Fidelity Index	10.1	9.4	16.5	18.4	17.4	18.4	23.3

Table 6.   Image qualities of simulation results using smoothed total power data for noisy cases (Object flux = 0.26 Jy).
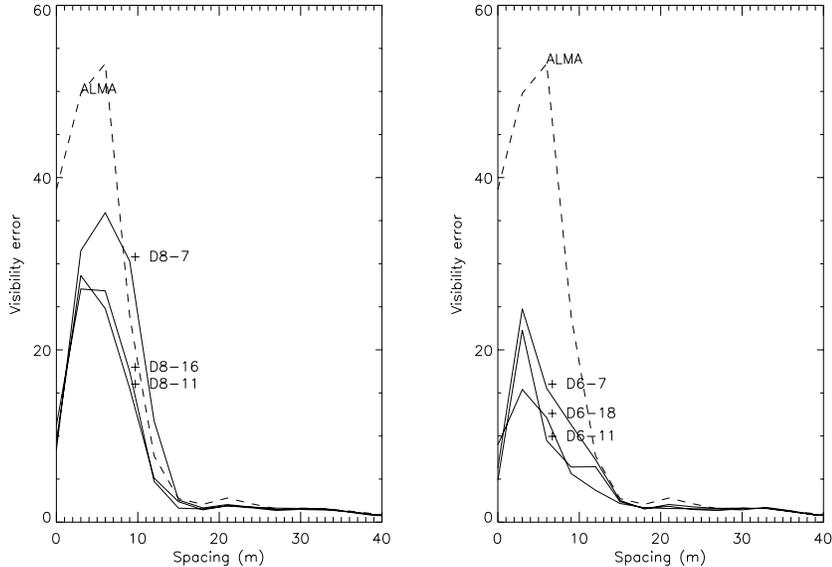
8

Figure 7.   Visibility error profile for noise free cases in Table 5.

In Table 5, most of imaging qualities for the cases using the ACA with 6 m antennas are superior to those for the ACA with 8 m antennas. The same tendency is also seen in Table 6, while the sensitivity of 8 m antennas is better than that of 6 m antennas. However, differences between these results using 6 m antenna and 8 m antenna are very small for noisy cases except for the ACA D8-7.

6.   Discussion

6.1.   The optimum design

In Table 5 and Table 6, most of imaging qualities for the cases of the ACA with 6 m antennas are superior to those for the ACA with 8 m antennas. This fact is consistent with discussion of sensitivity response patterns of the ALMA and the ACA in (u,v) plane. The peak of the responses of the ACA with 6 m antennas is almost at the center of the (u,v) hole as shown in Figure 9 (b). For the case of 8 m antennas, the peak is at the edge of the (u,v) hole as shown in Figure 9 (a). Therefore, the ACA with 8 m antennas is not so efficient to compensate this (u,v) hole compared with 6 m antennas.

The larger diameter is desirable for accurate calibrations. For the ACA with more than 10 antennas, differences between image qualities using 6 m and 8 m are small especially for noisy cases. Therefore, if we cannot always use cross correlations between the ACA and the ALMA for calibrations, design of more than 10 × 8 m antennas is desirable for the ACA.

6.2.   Joint deconvolution software

In section 5.1, we show that it is hard to obtain significant improvement by adding ACA data simply to ALMA data. One reason is because the long Fourier information in the total power from the 12 m antennas suffers from phase errors due to the pointing errors, and the 12 m total power data actually has more sensitivity in the 6-8 m range than the ACA interferometric measurements have. Dyanmic ranges, however, are almost same for all cases using different number of smaller antennas. This fact is difficult to explain only by the sensitivity discussion.
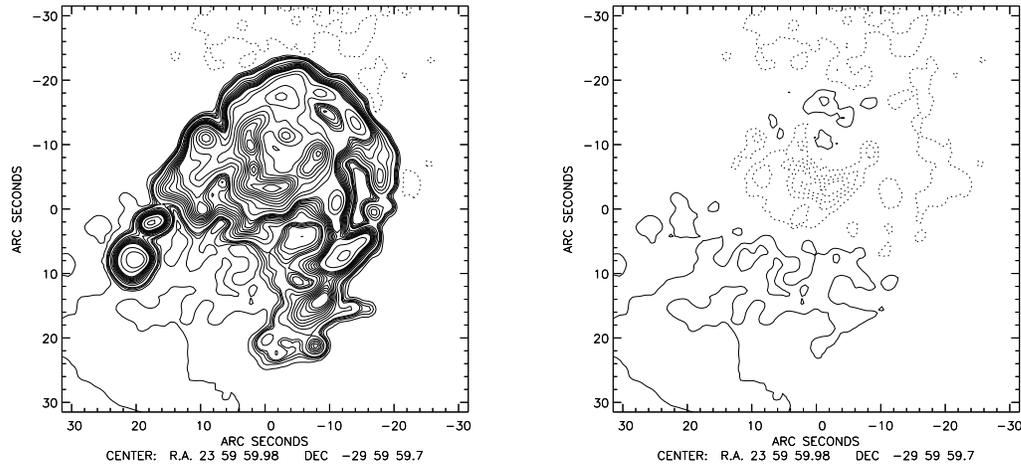
9

Figure 8.   Left (a): The deconvolved image for the pointing error with 6.1 % of primary
beam width of 12 m atenna. CContours = [-1, -0.8, -0.6, -0.4, -0.2, 0.2, 0.4, 0.6, 0.8, 1,
2, 3, 4, 5, 6, 7, 8, 9, 10, 15, 20, 30, 40, 50, 60, 70, 80, 90] % The error distribution of the
image in Figure 3. Right (b): Contour interval is 0.2 % of the peak.
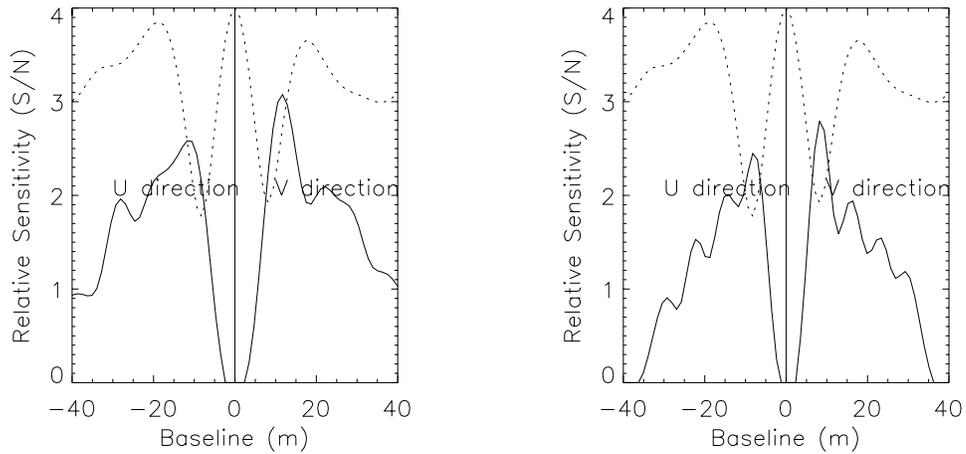

Figure 9.   Left (a): Sensitivity profiles of the ALMA (Dot) and the ACA D8-16 (Solid).
Right (b): Sensitivity profiles of the ALMA (Dot) and the ACA D6-18 (Solid).

10

Joint deconvolution algorithm used in these simulations is based on Maximum Entropy Method. In this algorithm, we need to calculate chi squares for each pointing and obtain a weighted sum. We have experienced that resultant image qualities are very sensitive to the weights. The deconvolution software used in these studies could be not optimaized for such heterogeneous array data and above facts might be due to such an incompleteness of the weighting treatment.

We probably need to repeat same set of simulations using different softwares (for example: AIPS++) or algorithms.

6.3.   Another option

In Figure 3, imaging quality decreases very fast as the pointing errors increase. For noise free cases, dynamic ranges at 3 % and 6 % of FWHM of the 12 m antenna beam pattern are about 800 and 400, respectively. It means that, if we can make the pointing accuracy of the 12 m antennas two times accurate, the imaging performance of the ALMA becomes almost two times better. Therefore, making all or several 12 m antennas very high accurate is another option to realize high fidelity imagings for large objects. To chose which option would depend on the cost.

7.   Summary

- Antenna pointing errors are a serious problem for obtaining high quality images for large scale objects with ALMA, because it makes a large error in visibility in the (u,v) hole.

- The ACA which consists of several smaller dishes (6-8m) can compensate this problem. However, to obtain higher image quality, we need a low pass filtering of the total power data in adding process of the ACA data to the ALMA data.

- The ACA with 6 m antennas has better imaging performance than the ACA with 8 m antennas, but the difference between them is small for noisy cases.

- Improving the pointing accuracy of all or some of the 12 m antennas is another option to realize high fidelity imaging for large objects.

Reference

Cornwell, T. J., Holdaway, M. A., and Uson, J. M., 1993, *A. & Ap.* 271, 697.
Ekers, R. D., and Rots, A. H., 1979, In: C. van Schooneveld (ed.), *Proc. IAU Col. 49*,
        D. Reidel, 61.
Yun, M. S., 2001, *ALMA memo* No. 368.